



REINFORCED CONCRETE BRIDGE COLUMNS TESTED UNDER LONG AND SHORT-DURATION GROUND MOTIONS

M. Mohammed⁽¹⁾, D. Sanders⁽²⁾, and I. Buckle⁽³⁾

⁽¹⁾ PhD Candidate, University of Nevada, Reno, mohammed@nevada.unr.edu

⁽²⁾ Professor, University of Nevada, Reno, sanders@unr.edu

⁽³⁾ Professor, University of Nevada, Reno, igbuckle@unr.edu

Abstract

Recent earthquakes in Indonesia (2004), Chile (2010), and Japan (2011) are reminders of the possible occurrence of a long-duration, large-magnitude earthquake in the Cascadia subduction zone along the Pacific Northwest Coast of the United States. The importance of studying the effect of ground motion duration on structural performance has been highlighted by these earthquakes. Current seismic design specifications do not consider this effect. Conclusions from previous research with regard to duration have been conflicting. This paper describes a comprehensive experimental study to investigate the effect of duration on reinforced concrete (RC) bridge columns. The results of shake table tests of three identical large-scale RC bridge columns are discussed. The columns were tested using spectrally equivalent long and short-duration ground motions. A cumulative damage metric is used to define columns damage states. This metric was correlated against damage states obtained from published data on more than 25 bridge columns that had been tested to failure. The results showed that the columns subjected to long-duration motions were more highly damaged than those with short-duration motions. The reinforcing steel in the columns subjected to longer motions had a significantly larger number of plastic strain cycles, which caused the bars to fracture at lower displacements compared to the columns subjected to short-duration motions; i.e. ground motion duration affected the collapse capacity of these columns. Therefore, it is recommended that duration effects be considered in the seismic design of bridges, especially in regions where long-duration earthquakes may occur.

Keywords: ground motion duration; shake table experiments; bridge columns; reinforced concrete

1. Introduction

Long-duration earthquakes that have occurred in Chile in 2010, 2014 and 2015, Japan in 2011, China in 2008, and Indonesia in 2004 are reminders of the importance of the effect of ground motion duration on structural response. Many monitoring stations across Japan recorded ground motions lasting from 50-270 seconds (total duration) during the Tohoku 2011 earthquake. On the other hand, ground motion durations measured in California typically last less than 30 seconds. The fault size for the Tohoku earthquake was about 500 km x 200 km. Anderson [1] suggests that a shallow dip to the subducted slab permits abundant earthquakes based on the evidence that the Tohoku earthquake occurred on a shallow-dipping fault before the subduction angle becomes steep. Thus, a similar scenario might be repeated in the Cascadia subduction zone. Most current seismic design specifications use response spectra to specify the hazard and do not consider duration effects. This might be attributed to the lack of available long-duration ground motion records, which has led researchers to rely primarily on simulated records. The variation in conclusions of previous research [2], with regard to the effect of strong ground motion duration on structural performance, might also be another reason for why existing specifications do not consider duration effects.

The influence of duration on structural performance depends on the damage metric used, the duration definition, and on the structural model [2]. Studies that use peak response have generally found no correlation between ground motion duration and structural damage [3,4]. However, studies that use cumulative damage measures [4] or energy measures [3, 4] have found a correlation between duration and damage. Boomer and Martinez-Pereira [5] report many definitions of strong ground motion duration from the literature. Arias Intensity [6] and Cumulative Absolute Velocity [7] can be used as metrics for duration. These are measures of the energy content of a ground motion. Arias Intensity (AI) is defined as the integral of the square of the

acceleration history over time. Cumulative Absolute Velocity (CAV) is defined as the integral of the absolute value of the acceleration history over time. Two additional popular duration definitions are the bracketed and the significant durations. The bracketed duration is defined as the measure of the time interval between the first and last exceedance of an absolute acceleration threshold; typically 0.05g or 0.1g. The significant duration is defined as the interval over which a specific amount of Arias Intensity is achieved; this amount is usually taken as 5% to 95% or 5% to 75% of the Arias Intensity.

2. Test specimens, setup, and loading protocol

The test specimens and setup for this study were adopted from a previous study by Phan et al. [8], where a 1/3-scaled bridge column, designated as NF-2, was tested using the Rinaldi ground motion until failure. A previous test was selected to utilize the readily available damage states and maximum displacement capacity, 9.8 in., in finalizing the ground motion selection and spectral matching for this experimental program as discussed in a following section. Three identical reinforced concrete (RC) column specimens were constructed with similar details as NF-2 [8]. The height of each column was 72 in.; the diameter was 16 in.; the longitudinal reinforcement was 22 #4 bars; the transverse reinforcement was a 0.25-in. steel wire spiral with a 1.25 in. pitch; the axial load ratio was 8% of the column axial capacity; and the clear cover was 0.75 in. Specimen details and dimensions are shown in Fig. 1a.

All columns were tested on one of the four shake tables in the Earthquake Engineering Laboratory at the University of Nevada, Reno. The top of each specimen was attached laterally to an 80-kip weight to represent the inertial mass of the bridge superstructure as shown in Fig. 1b. The ground motions were uniaxial and applied along the North-South direction of the laboratory. The three column specimens are designated as LD-J1, LD-J2, and SD-L to indicate two long-duration tests using two different Japan earthquake records and one short-duration test that used a ground motion from the Loma Prieta earthquake (details are discussed in next section). Multiple instruments were used to monitor each specimen including strain gauges, LVDT's, string potentiometers, displacement transducers, accelerometers, and high definition video cameras. Columns LD-J1, SD-L and LD-J2 began with 100% of the selected motions then followed by an aftershock. The main motions were then incrementally amplified until failure (125%, 150%, ..., and so on). The applied aftershocks were chosen from the M_w 7.1 earthquake that occurred in Japan one month after the Tohoku earthquake.

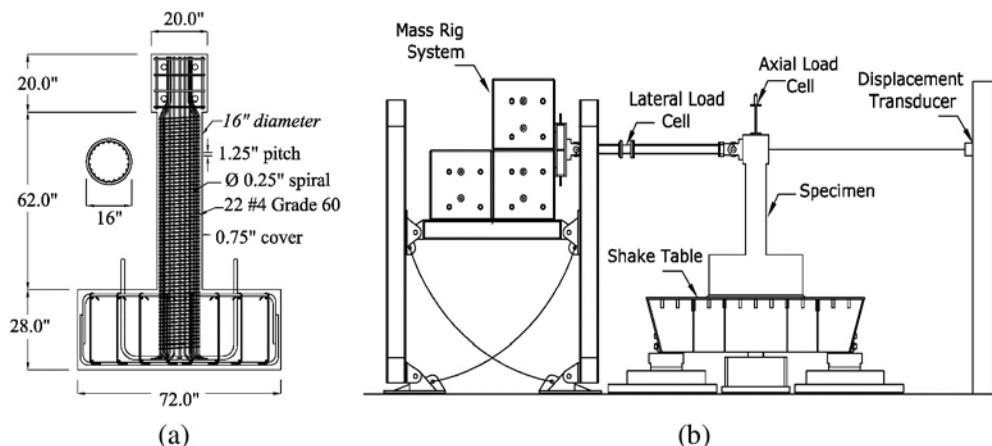


Fig. 1 – (a) Specimen details and dimensions (b) Test setup

3. Pre-test analysis and ground motion selection

The main objectives of the pre-test work were to choose ground motions for the experimental program and to estimate the dynamic response of the test specimens, as discussed in this section. Moreover, a fragility-based framework was used for damage prediction as discussed in the next section.

3.1 Model Calibration

To finalize the selection of input ground motions for the experimental program, a detailed OpenSees [9] pre-test analysis was conducted. The main goal was to choose ground motions in which the displacement demands on the columns are much less than the 9.8 in. displacement capacity determined from Phan et al. [8]. The RC column was modeled using a fiber cross section and a force-based beam-column element with distributed plasticity. The Concrete01 material was used to represent the stress-strain relationship of concrete, and the Steel02 material was used to represent the longitudinal reinforcement. The analytical model was calibrated using the results from Phan et al. [8]. A simple illustration of the model and the comparison between the experimental and analytical force-displacement relationship are shown in Fig. 2. The good match between the calibrated model and experimental results gave confidence for utilizing the model in ground motion selection

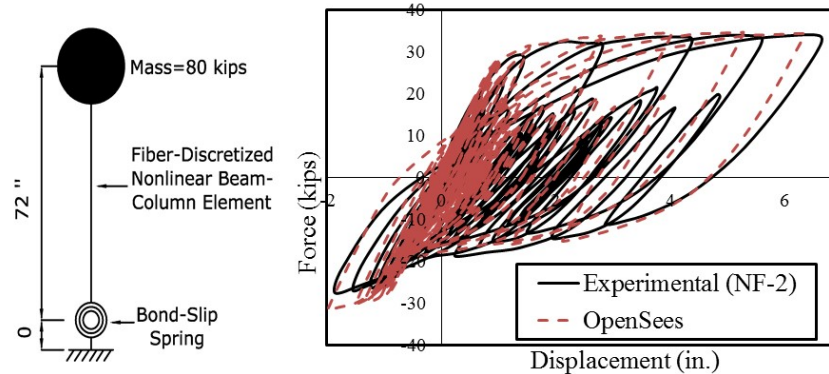


Fig. 2 – OpenSees model description and results compared to NF-2 [8] experimental test

3.2 Ground motion selection

An inventory of ground motion records was assembled from several large-magnitude long-duration earthquakes including the 2011 Tohoku, Japan earthquake, the 2010 Maule, Chile earthquake, and the 2008 Wenchuan, China earthquake. Note that the 2008 Wenchuan, China earthquake was also long duration although it was not a subduction event. Short duration motions were also collected from the PEER-NGA database. Based on the calibrated OpenSees model, a long-duration motion from the Tohoku 2011 earthquake (FKSH20 N-S) was chosen for Column LD-J1, and a short-duration motion from the Loma Prieta 1989 earthquake (BRAN 00) was chosen for Column SD-L. Figure 3 shows the 2475 year response spectra for different cities from the Northwest of the United States that lie near the Cascadia subduction zone (site class D). These response spectra were based on the USGS Hazard Curves [10]. The selected motions for Columns LD-J1 and SD-L had to be modified to get the target displacement demands. The motions were modified to match the response spectra shown in Fig. 3. After comparing the results of the different modified motions from the OpenSees analysis, Crescent City response spectrum was chosen to be the target spectrum and the original motions were finalized accordingly. The spectral matching for these two motions (LD-J1 and SD-L) was done for a period range from 0.5 to 3 seconds. The target was to impose maximum displacement demands on the two specimens with around half of the maximum displacement capacity which is 9.8 in. (known before testing from Phan et al. [8]), and since the two motions have a similar spectral shape, the difference between them was their durations. For Column LD-J2, another long-duration motion from the Tohoku earthquake was chosen (MYG006 E-W). The motion was not modified, but it was chosen because its response spectrum was as close as possible to the final motions used for Columns LD-J1 and SD-L. The response spectra of the selected motions, the modified acceleration histories (LD-J1 and SD-L), and the actual record for LD-J2 are shown in Figs. 4, 5, and 6, respectively.

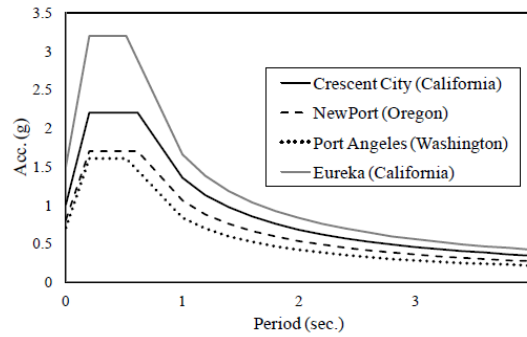


Fig. 3 – Response spectra (2475 year return period) for different cities (USGS-site class D)

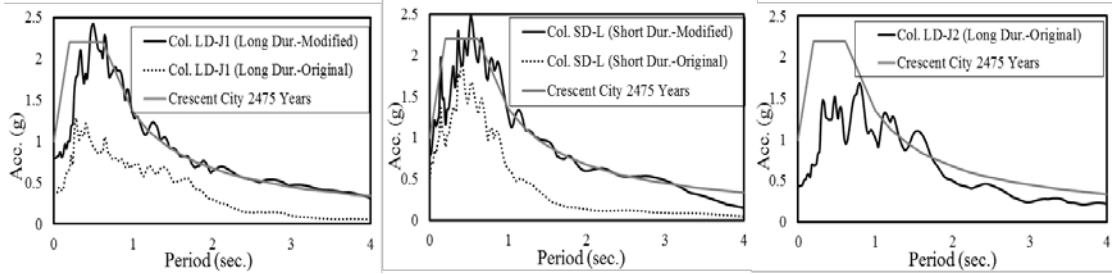


Fig. 4 – Response spectra of the long and short-duration motions (5% damping)

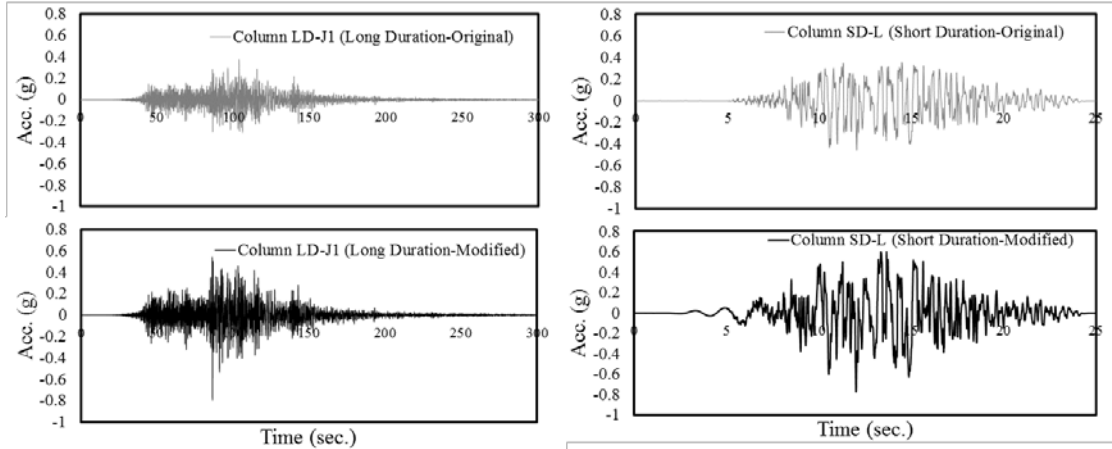


Fig. 5 – Acceleration histories for long and short-durations motion before and after spectral matching; Column LD-J1 (left set) and Column SD-L (right set)

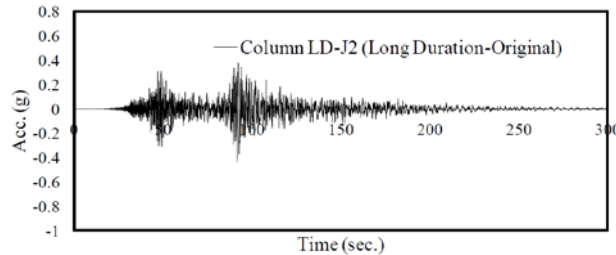


Fig. 6 – Acceleration history for the long-duration motion (Column LD-J2)

The time scale of the selected ground motions was compressed using a factor of 0.577 to take into account the scaling from the prototype to the model (1/3 scale). For a convenient comparison, the three final motions response spectra are shown in Fig. 7. Moreover, the four duration metrics previously identified: the significant duration, bracketed duration, AI, and CAV were computed for the final motions as summarized in Table 1.

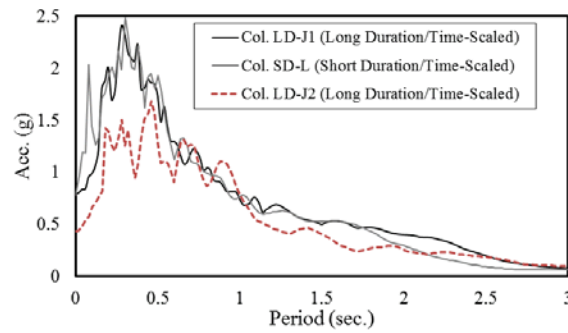


Fig. 7 – Response spectra of the final, time-scaled long and short-motions used in the project (5% damping)

Table 1 – Summary of the duration metrics for the selected ground motions

Target Motion		Significant duration (5%-95% of AI) (seconds)	Significant duration (5%-75% of AI) (seconds)	Arias Intensity (AI) (cm/sec.)	CAV (cm/sec.)	Bracketed duration (0.1g threshold) (seconds)
Col. LD-J1 (Long Dur.) (100%)	Original	88.3	57.9	2704	11768	110.72
	Time-scaled	50.95	33.42	1560	6790	63.88
Col. SD-L (Short Dur.) (100%)	Original	9.1	5.9	1098	2621.3	16.55
	Time-scaled	5.23	3.39	633	1510	9.53
Col. LD-J2 (Long Dur.) (100%)	Original	115	57.96	1352	9015	114.2
	Time-scaled	66.39	33.44	780	5202	65.93

3.3 Pre-test analysis

Pre-test analysis was done using the calibrated OpenSees model and by applying the chosen motions using the same loading protocol as discussed above. The force-displacement relationships for the three models using 100% of the target motions are shown in Fig. 8, where it will be seen that the maximum displacements for the three models are almost the same. Consequently, the three ground motions are treated in the same way by the seismic design specifications where they neglect the large number of inelastic cycles imposed on the columns by the long-duration motions. More details about the expected damage for the columns are discussed in the next section.

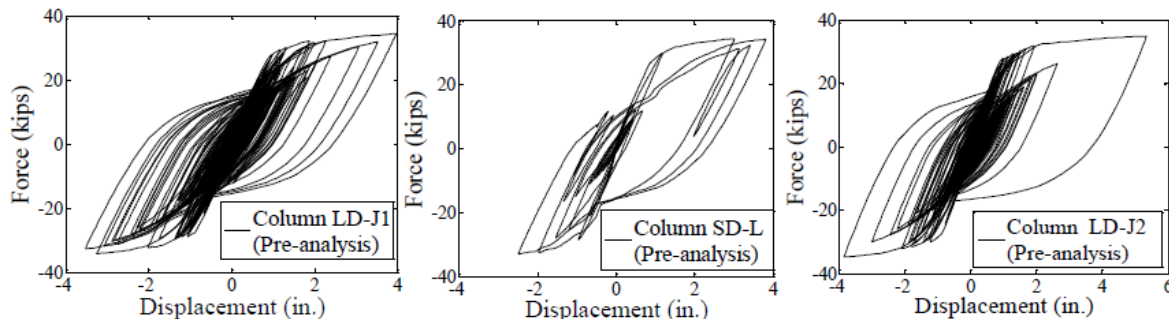


Fig. 8 – Pre-test analysis results (force-displacement) using 100% of the selected motions

4. Fragility curves and expected damage

In the second phase of the pre-test work, experimental fragility curves were developed from published test data to utilize along with the cumulative damage index to predict the expected damage for the three columns considered in this study.

4.1 Cumulative damage index

Park and Ang [11] expressed seismic damage as a linear combination of the damage caused by the maximum deformation and by the cumulative damage resulting from the repeated cycles (Eq. 1). This damage index (DI) is used in this study to quantify the damage to the columns.

$$DI = \frac{\delta_m}{\delta_u} + \beta \frac{\int E_h}{F_y \delta_u} \quad (1)$$

where, δ_m = maximum displacement demand for a specific damage state, δ_u = ultimate displacement sustained by a column from an experimental test (modified from the original Park and Ang [11] definition), β = non-negative parameter representing the effect of cyclic loading and taken as 0.15 [12, 13, 14], F_y = yield force, and E_h = dissipated hysteretic energy.

4.2 Experimental fragility curves

Data from over 25 bridge column models that had been tested on shake tables or under lateral quasi-static loads [8, 15, 16, 17, 18, 19, 20, 21, 22, 23] were used to develop experimental fragility curves. The column models used were designed based on modern seismic design specifications. The fragility analysis approach was used to correlate the Park and Ang damage index, with the modified δ_u definition, with five apparent damage states (Fig. 9) for bridge columns. The fragility functions took the form of lognormal cumulative distribution functions, and considered the effect of scatter in the data as illustrated in Fig. 9.

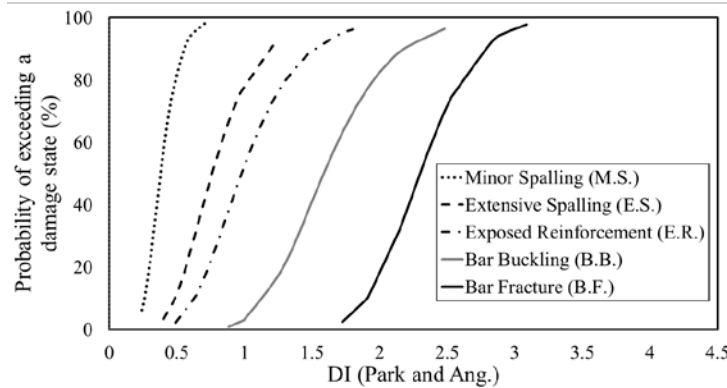


Fig. 9 – Experimental fragility curves correlating damage index (DI) with different damage states

4.3 Expected performance of the columns

As mentioned before, a pre-test analysis for the three columns was done using the calibrated OpenSees model. The Park and Ang damage index was calculated after each motion. The analytically calculated damage index and the experimental fragility curves were used to predict the performance and the damage for the columns as summarized in Table 2. The columns that were subjected to long-duration motions were expected to experience more damage and to fail at a lower level of the main motion compared to the column that was subjected to the short-duration motion.

Table 2 – Estimated performance of the test columns

Specimen		100% of the motion	Aftershock	125% of the motion	150% of the motion	175% of the motion
LD-J1	DI	1.37	1.5	2.94		
	Expected performance	- 29% B.B. - 84% E.R.	- 40% B.B. - 89% E.R.	- 95% B.F. - 100% B.B.		
SD-L	DI	0.542	0.69	1.14	1.71	2.53
	Expected performance	- 2.5% E.R. - 12% E.S. - 83% M.S.	- 15% E.R. - 40% E.S. - 97 % M.S.	- 8% B.B. - 63% E.R. - 84% E.S.	- 60% B.B. - 95% E.R.	- 74% B.F. - 100% B.B.
LD-J2	DI	1.243	1.347	2.27		
	Expected performance	- 17% B.B. - 77% E.R. - 100% E.S.	- 22% B.B. - 82% E.R. - 100% E.S.	- 50% B.F. - 92% B.B.		

Refer to Fig. 9 for definitions of the five damage states: B.F., B.B., E.R., E.S., and M.S.

5. Test results and discussions

Selected results that included shake table accelerations, visual damage, force-displacement relationships, and reinforcement strains from the three column tests are presented and discussed in this section.

5.1 Shake table fidelity

To test the fidelity of the shake table, the desired input acceleration record (target) was compared against the actual acceleration achieved (feedback) by the shake table. Fig. 10 shows the 5%-damping response spectra comparison of the target and feedback accelerations for the 100% scale considered ground motions. A good match was observed in each case over the range of periods of interest. Moreover, Fig. 11 shows that the response spectra of the recorded accelerations for the three columns are almost the same. Thus, the variation in dynamic response should be attributed primarily to the ground motion duration.

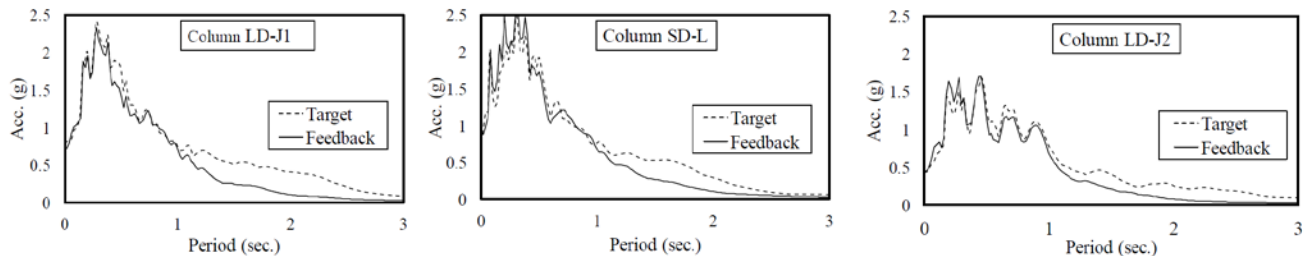


Fig. 10 – Feedback versus target response spectra (5% damping) for 100% scale ground motions

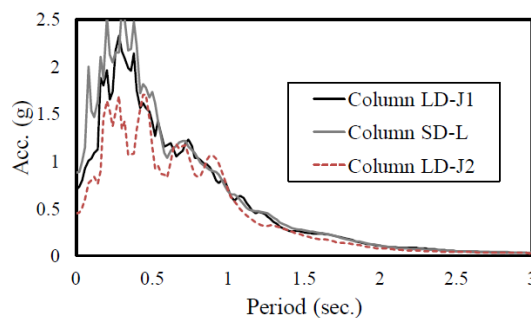


Fig. 11 – Feedback response spectra (5% damping) for the recorded 100% scale ground motions for the three column tests

5.2 Damage description

The damage states of the three columns were compared using both visual observations and computed damage indices. Table 3 compares the predicted pre-test and the actual post-test damage indices and damage states for the columns. More details on the observed damage are discussed for the three columns in Table 4. Column LD-J1 and Column LD-J2, which were subjected to long-duration motions, reached their final damage states at 125% scale of the ground motion. This corresponded to four longitudinal bars ruptures in Columns LD-J1 and one rupture in LD-J2. However, the failure of Column SD-L under the short-duration motion, occurred at 175% scale of the ground motion with one bar fractured. Fig. 12 shows the damage states for the three specimens after the 125% scale tests.

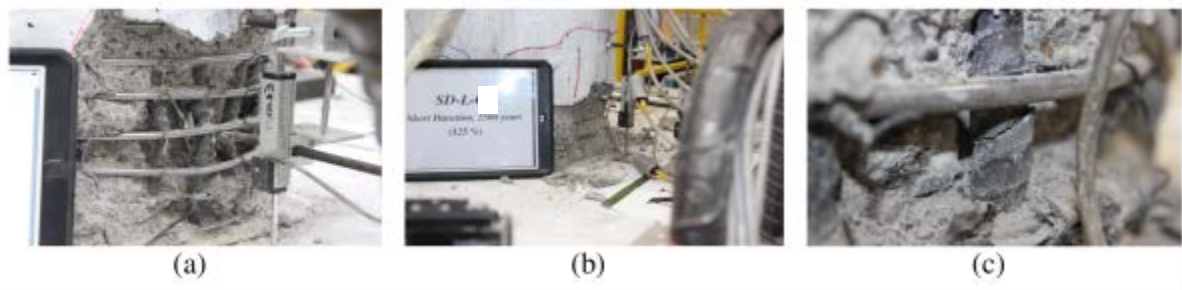


Fig. 12 – Damage states after applying 125% of the main motion for: (a) Column LD-J1; (b) Column SD-L; and (c) Column LD-J2

5.3 Hysteretic behavior and response histories

The measured force-displacement hysteretic curves for the three specimens are shown in Fig. 13. The maximum displacement for Column LD-J1, Column SD-L, and Column LD-J2 was 4.98 in. (at 125% of the target motion), 9.2 in. (at 175% of the target motion), and 7.4 in. (at 125% of the target motion), respectively. The maximum displacement demands for Columns LD-J1 and LD-J2 were less than the displacement capacity, which was reached in Column SD-L test. Accordingly, the failure in LD-J1 and LD-J2 can be attributed to the large number of applied cycles, which indicates that long-duration motions can be more damaging than short-duration ones.

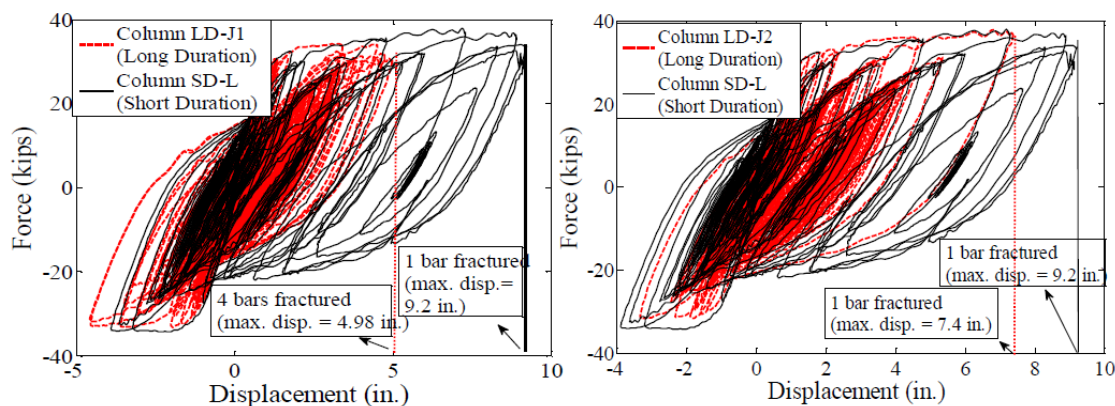


Fig. 13 – Comparison of the total cumulative force-displacement hysteretic curves (Columns LD-J1 and LD-J2 with Column SD-L)

Strain histories for the three specimens after applying 100% of the main motion are shown in Fig. 14a. The histories are for strain gauges at 4 inches above the footings. The longitudinal bars in Columns LD-J1 and LD-J2 were subjected to a large number of high-strain cycles compared to Column SD-L. This shows the significant effect of the large number of inelastic cycles on the collapse capacity of the columns. Figure 14b shows the

displacement histories for Columns LD-J1 and LD-J2 for the 125% of the main motion when fracture of the longitudinal bars occurred. It is worth noting that fracture did not occur at the maximum displacement demands (see Fig. 14b).

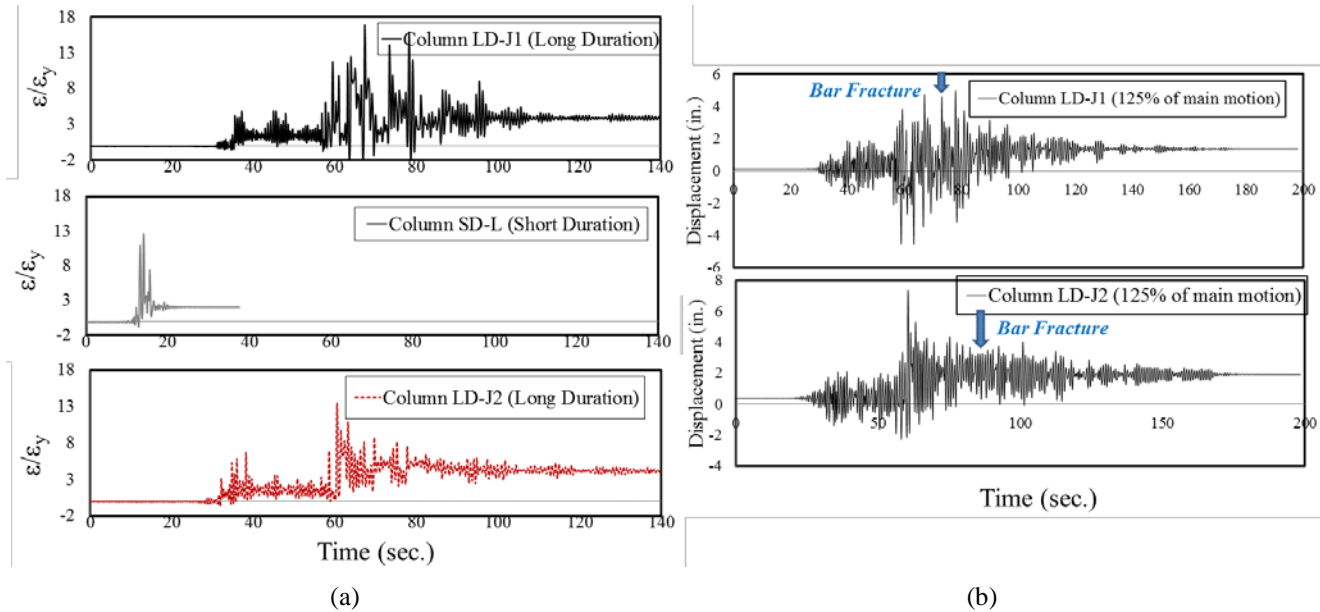


Fig. 14 – (a) Strain histories for the three specimens measured at 4 inches above the footings; (b) displacement histories for the 125% motion for the long-duration motions

5.4 Spectral accelerations at failure

The actual shake table acceleration response spectra were compared for the motions when the columns reached their final damage states. The response spectra comparison of these accelerations is shown in Fig. 15. Columns LD-J1 and LD-J2 failed at 125 % scale of the main motion. Column SD-L failed at 175 %. The spectral acceleration at failure for the columns subjected to long-duration motions are about 40% less than the column subjected to the short-duration motion (Fig. 15).

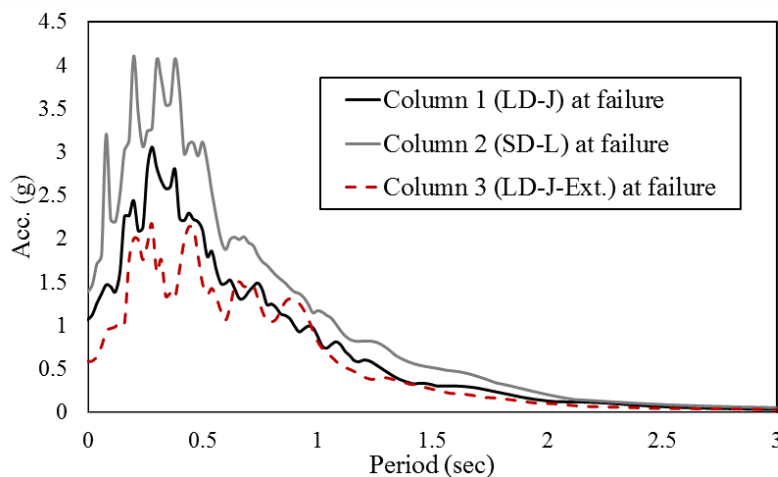


Fig. 15 – Response spectra at final damage state for the three columns



Table 3 – Pre- and post-test comparison

Specimen		100% of the motion	Aftershock	125% of the motion	150% of the motion	175% of the motion
LD-J1	DI (pre-test analysis)	1.37	1.5	2.94		
	Expected performance	- 29% B.B. - 84% E.R.	- 40% B.B. - 89% E.R.	- 95% B.F. - 100% B.B.		
	DI (test)	1.33	1.45	2.44		
	Actual damage	- E.R.	- E.R.	- B.F.		
SD-L	DI (pre-test analysis)	0.542	0.69	1.14	1.71	2.53
	Expected performance	- 2.5% E.R. - 12% E.S. - 83% M.S.	- 15% E.R. - 40% E.S. - 97% M.S.	- 8% B.B. - 63% E.R. - 84% E.S.	- 60% B.B. - 95% E.R.	- 74% B.F. - 100% B.B.
	DI (test)	0.55	0.67	0.99	1.6	2.26
	Actual damage	-M.S.	-M.S.	-E.R.	-E.R.	-B.F.
LD-J2	DI (pre-test analysis)	1.243	1.347	2.27		
	Expected performance	- 17% B.B. - 77% E.R. - 100% E.S.	- 22% B.B. - 82% E.R. - 100% E.S.	- 50% B.F. - 92% B.B.		
	DI (test)	1.19	1.34	2.48		
	Actual damage	- E.R.	- E.R.	- B.F.		

Refer to Fig. 9 for definitions of the five damage states: B.F., B.B., E.R., E.S., and M.S.

Table 4 – Comparison of the actual damage states between the tested columns

Applied Motion	Actual Damage State		
	Column LD-J1	Column SD-L	Column LD-J2
100% of the main motion	-Max. Disp. = 4.5 in. -South: 4.4 in. spalling and the spirals are exposed. -North: 3.0 in. spalling and the spirals are exposed.	-Max. Disp. = 3.88 in. -South: cracks of max. width of 0.016 in. -North: 4.5 in. spalling and no exposed reinforcement.	-Max. Disp. = 4.7 in. -South: 7.5 in. spalling and the spirals are exposed. -North: 2.0 in. spalling and no exposed reinforcement.
Aftershock	-Same visual damage state as the previous motion.	-Same visual damage state as the previous motion.	-Same visual damage state as the previous motion.
125% of the main motion	-Max. Disp. = 4.98 in. -South: 8.5 in. spalling and four longitudinal bars fractured (failure). -North: 6.4 in. spalling and the concrete core is damaged.	-Max. Disp. = 4.8 in. -South: 4.5 in. spalling and the spirals are exposed. -North: 4.5 in. spalling and the spirals are exposed.	-Max. Disp. = 7.4 in. -South: 8.0 in. spalling and three longitudinal bars buckled. -North: 5.0 in. spalling and one longitudinal bar fractured (failure).
150% of the main motion	-Not applicable as bars fractured at 125% of the main motion.	-Max. Disp. = 7.3 in. -South: 9.0 in. spalling and the spirals are exposed. -North: 6.0 in. spalling and the spirals are exposed.	-Not applicable as fracture occurred at 125% of the main motion.
175% of the main motion	-Not applicable as bars fractured at 125% of the main motion.	-Max. Disp. = 9.2 in. -South: four longitudinal bars buckled. -North: one longitudinal bar fractured and two buckled.	-Not applicable as fracture occurred at 125% of the main motion.



6. Conclusions

This paper described an experimental study investigating the effect of ground motion duration on structural performance of RC bridge columns. Experimental fragility curves were developed that correlate a cumulative damage index with different damage states. These curves were used to predict the performance of bridge columns subjected to long-duration motions in a probabilistic approach. From the shake table test results, a significant reduction in the displacement capacity was observed for the columns that were subjected to long-duration motions compared to the one subjected to the short duration. The spectral acceleration for the long-duration motions that caused collapse were about 40% less than that of the short-duration motion at collapse. The accumulated plastic strains in the reinforcing bars of the columns subjected to long motions caused the bars to fracture early even if the maximum displacement demands were low. Based on these results, ground motion duration is considered to have a significant effect on the collapse capacity of bridge columns. Therefore, it is recommended to consider the effect of duration in seismic design provisions for bridges, or when choosing ground motions for nonlinear history analysis for bridges, especially in regions where long-duration earthquakes are expected to occur.

7. Acknowledgements

The study presented in this paper was funded by the Federal Highway Administration under Contract No. - DTFH61-07-C-00031. Acknowledgement is made of the oversight given by the Contract Officer's Representatives: Dr. Wen-huei (Phillip) Yen, Mr. Fred Faridazar, and Ms Sheila Duwadi. The authors would also like to thank Dr. Patrick Laplace, Chad Lyttle and Todd Lyttle for their help during the experiments. The conclusions and findings in this paper are those of the authors and do not necessarily represent the views of the funding agency.

8. References

- [1] Anderson, J. G. (2013): Surface motions on near-distance rock sites in the 2011 Tohoku-Oki earthquake. *Earthquake Spectra*, **29**(S1), S23-S35.
- [2] Hancock, J., and Boomer, J. J. (2006): A State-of-knowledge review of the influence of strong-motion duration on structural damage. *Earthquake Spectra*, **22**(3), 827-845
- [3] Iervolino, I., Manfredi, G., and Cosenza, E. (2006): Ground motion duration effects on nonlinear seismic response. *Earthquake Eng. Struct. Dyn.*, **35**(1), 21-38.
- [4] Hancock, J., and Boomer, J. J. (2007): Using spectral matched records to explore the influence of strong-motion duration on inelastic structural response. *Soil Dyn. Earthquake Eng.*, **27**(4), 291-299.
- [5] Bommer, J. J., and Martinez-Pereira, A. (1999): The effective duration of earthquake strong motion. *Journal of Earthquake Engineering*, **3**(2), 127-172.
- [6] Arias, A. (1970): A measure of earthquake intensity. *Seismic Design for Nuclear Power Plants*, edited by R. J. Hansen, MIT Press, Cambridge, MA, pp. 438-489.
- [7] Benjamin, J. R. (1988): A criterion for determining exceedance of the operating basis earthquake. *EPRI Report NP-5930*. Electric Power Research Institute, Palo Alto, CA.
- [8] Phan, V., Saiidi, M. S., and Anderson, J. (2005). Near fault (near field) ground motion effects on reinforced concrete bridge columns. *Report No. CCEER-05-07*, Center for Civil Engineering Earthquake Research, University of Nevada Reno, Reno, NV.
- [9] McKenna, F., Fenves, G.L. and Scott, M.H. (2006): OpenSees: Open System for Earthquake Engineering Simulation, Pacific Earthquake Engineering Research Center, University of California Berkeley, Berkeley, CA., <http://opensees.berkeley.edu>.
- [10] United States geological survey (2014), <http://www.usgs.gov/>.
- [11] Park, Y., and Ang, A. H. (1985): Mechanistic seismic damage model for reinforced concrete. *J. Struct. Eng.* **111**(4), 740-757.



- [12] Fajfar, P. (1992): Equivalent ductility factors, taking into account low-cycle fatigue. *Earthquake Engineering & Structural Dynamics*, **21** (10), 837-848.
- [13] Cosenza, E. Manfredi, G., and Ramasco, R. (1993): The use of damage functionals in earthquake engineering: a comparison between different methods. *Earthquake Engineering & Structural Dynamics*, **22** (10), 855-868.
- [14] Karim, K., and Yamazaki, F. (2001): Effect of ground motions on fragility curves of highway bridge piers based on numerical simulation. *Earthquake Engineering & Structural Dynamics*, **30** (12), 1839-1856.
- [15] Cheok, G. S., and Stone, W. C. (1986): Behavior of 1/6-Scale model bridge columns subjected to cycle inelastic loading; *NBSIR 86-3494*, Center for Building Technology, National Engineering Laboratory, National Institute of Standards and Technology.
- [16] Stone, W. C., and Cheok, G. S. (1989): Inelastic behavior of full-scale bridge columns subjected to cyclic loading. *NIST BSS 166*, Building Science Series, Center for Building Technology, National Engineering Laboratory, National Institute of Standards and Technology.
- [17] Kunnath, S. K., El-Bahy, A., Taylor, A., and Stone, W. (1997): Cumulative seismic damage of reinforced concrete bridge piers. *Technical Report NCEER-97-0006*, National Center for Earthquake Engineering Research.
- [18] Lehman, D. E., and Moehle, J. P. (2000): Seismic performance of well-confined concrete bridge columns. *Technical Report PEER 1998/01*, Pacific Earthquake Engineering Research Center, Berkeley, USA.
- [19] Calderone, A. J., Lehman, D. E., and Moehle, J. P. (2001): Behavior of reinforced concrete bridge columns having varying aspect ratios and varying lengths of confinement. *Technical Report PEER 2000/08*, Pacific Earthquake Engineering Research Center, Berkeley, USA.
- [20] Moyer, M. J. and Kowalsky, M.J. (2003): Influence of tension strain on buckling of reinforcement in RC bridge columns. *ACI Structural Journal*, **100**(1), 75-85.
- [21] Saiidi, M., and Mortensen, J. (2002): A new performance-based design for spirals in bridge columns. *Proceedings, The 7th U.S. Conference on Earthquake Engineering*, Boston, MA, USA.
- [22] Laplace, P., Sanders, D., and Saiidi, M. (1999): Shake table testing of flexure dominated reinforced concrete bridge columns. *Technical Report No. CCEER-99-13*, Center for Civil Engineering Earthquake Research, University of Nevada Reno, Reno, NV.
- [23] Schoettler, M., J., Restrepo, J., I., Guerrini, G., Duck, D., E., and Carrea, F. (2015): A full-scale, single-column bridge bent tested by shake-table excitation. *Technical Report PEER 2015/02*, Pacific Earthquake Engineering Research Center, Berkeley, USA.